Effect of Deformation Parameters on the No-Recrystallization Temperature in Nb-Bearing Steels

D.Q. BAI, S. YUE, W.P. SUN and J.J. JONAS

The recrystallization behavior of three Nb-bearing high-strength low-alloy (HSLA) steels was investigated during multipass deformation under continuous cooling conditions. The niobium concentrations of these steels varied from 0.05 to 0.09 wt pct. The specimens were tested on a computerized torsion machine using a simulation schedule of 17 passes. Deformation temperatures of 1180 °C to 700 °C were employed, together with pass strains of 0.1 to 0.7, strain rates of 0.2 to 10 s^{-1}, and interpass times of 5 to 200 seconds. By means of mean flow stress *vs* $1000/T$ diagrams, the effect of the deformation conditions on the no-recrystallization temperature (T_{nr}), the temperature at which recrystallization is no longer complete, was determined. It decreases with increasing strain and also decreases slightly with increasing strain rate. There is a T_{nr} minimum at times of about 12 ~ 15 seconds, and both increases and decreases from this value raise this characteristic temperature. When the interpass times are short, solute atoms control the rate of recrystallization, the extent of which decreases as the time is decreased. When the interpass times are long, precipitation takes place and retards recrystallization, so that the extent of softening decreases.

I. INTRODUCTION

KNOWLEDGE of the no-recrystallization temperature (T_{nr}) is important in the design of controlled rolling schedules, because it determines the temperature below which the pancaking strain is accumulated. Avoiding the partial recrystallization that takes place in its vicinity can also help in reducing the occurrence of duplex grain structures. It is well known that the precipitation of carbonitrides during hot deformation plays an important role in retarding recrystallization, and several compression techniques have been developed for following the progress of precipitation in both austenite[1] and ferrite[2] under isothermal deformation conditions. In the case of multipass deformation under continuous cooling conditions, the hot torsion test has been widely used to simulate industrial hot-rolling processes.[3–11] In the study described in this article, the latter kind of test was employed to investigate the effect of deformation parameters, such as the pass strain, strain rate, and interpass time, on the T_{nr} during multipass deformation. This demonstrated that a T_{nr} is obtained even in the absence of precipitation but that it increases as the interpass time is decreased, in opposition to the dependence obtained when precipitation is taking place.

The addition of titanium to Nb-bearing steels can influence the kinetics of Nb(C,N) precipitation and thus the kinetics of recrystallization. The undissolved TiN particles present prior to deformation can act as nucleation sites for austenite recrystallization,[12,13,14] thus leading to faster recrystallization kinetics. Fine freshly precipitated TiN particles, on the other hand, can act as nucleation sites for Nb(C,N) precipitation, which then accelerate the progress of precipitation. Two levels of titanium addition (0.007 and 0.026 wt pct) were employed to investigate this phenomenon; the results obtained enabled the influence of titanium on the precipitation of Nb(C,N) and therefore on the recrystallization of austenite to be clarified.

D.Q. BAI, Graduate Student, S. YUE, Associate Professor, and J.J. JONAS, Professor, are with the Department of Metallurgical Engineering, McGill University, Montreal, PQ, Canada H3A 2A7. W.P. SUN, formerly Research Associate, McGill University, Department of Metallurgical Engineering, is with the Department of Metals and Materials Engineering, The University of British Columbia, Canada.

Manuscript submitted December 17, 1992.

II. EXPERIMENTAL MATERIALS AND PROCEDURE

A. *Experimental Materials*

Three high-strength low-alloy (HSLA) steels, containing niobium concentrations of 0.05, 0.07, and 0.09 wt pct, were employed in this work. The chemical compositions of these steels are shown in Table I. The different combinations of niobium, carbon, and nitrogen concentration present in these steels made it possible to investigate the effect of supersaturation on the kinetics of Nb(C,N) precipitation.

The as-received plates were machined into torsion specimens with gage lengths of 22.4 mm and diameters of 6.3 mm. This specimen size was selected to allow rapid cooling after completion of the tests and also to allow a strain rate of 2 s^{-1} to be reached. For tests at strain rates of 5 ~ 10 s^{-1}, specimens with reduced gage lengths of 10.4 mm were used. The experiments were carried out on a servohydraulic, computer-controlled torsion machine equipped with a Research Incorporated radiant furnace controlled by a Leeds and Northrup (North Wales, PA) temperature programming system. The details of this apparatus are described elsewhere.[15] Oxidation of the specimens at the testing temperatures was prevented by passing a continuous flow of high-purity argon through the furnace.

The equilibrium solution temperatures for Nb(C,N) in

Table I. Chemical Compositions of the Investigated Steels in Weight Percent

Steel	C	Si	V	Mn	Mo	Ti	Al	Nb	N
A (0.05Nb)	0.125	0.33	0.155	0.43	0.17	—	—	0.05	0.005
B (0.07Nb)	0.04	0.31	0.003	1.67	0.20	0.026	0.038	0.07	0.01
C (0.09Nb)	0.04	0.27	—	1.53	0.14	0.007	—	0.09	0.008

the present materials were evaluated from the following equation given by Irvine *et al.*:[16]

$$\log [Nb]\left[C + \frac{12}{14}N\right] = 2.26 - \frac{6770}{T} \qquad [1]$$

These were estimated to be approximately 1240 °C, 1153 °C, and 1187 °C for steels *A*, *B*, and *C*, respectively. An austenitization temperature of 1250 °C was selected for all three steels, which is well above their individual solution temperatures.

B. *Testing Schedule*

Multipass torsion tests were carried out using the test parameters shown in Table II. Pass strains ranging from 0.1 to 0.7 were employed, together with strain rates from 0.2 to 10 s^{-1} and interpass times from 5 to 200 seconds. In any particular test, the pass strain, strain rate, and interpass time were held constant. Such a multipass testing schedule is illustrated schematically in Figure 1. After soaking at 1250 °C for 15 minutes, the specimens were cooled at a series of constant rates. Seventeen passes were applied in each case, and the temperature was decreased by 30 °C from pass to pass. Slower cooling rates were used in the case of the longer interpass times, and faster cooling rates were used in the case of the shorter interpass times. The cooling rates in the different tests are given by the relation

$$\alpha = \frac{30\ °C}{t} \qquad [2]$$

where t is the interpass time in seconds.

C. *Determination of the T_{nr}*

The mean flow stress pertaining to each pass was calculated from the flow curves (Figure 2) obtained in this way using the equation

$$\bar{\sigma}_{eq} = \frac{1}{\varepsilon_b - \varepsilon_a}\int_{\varepsilon_a}^{\varepsilon_b} \sigma_{eq} d\varepsilon_{eq} \qquad [3]$$

A typical dependence of mean flow stress on inverse absolute temperature is shown in Figure 3. The slope change allows the mean flow stress *vs* inverse temperature relation to be divided into two regions. In region I (which corresponds to high-temperature deformation), full recrystallization takes place; because there is no strain accumulation, the increase in mean flow stress is solely due to the decrease in temperature. In region II (which corresponds to deformation below the T_{nr}), there is only partial recrystallization or no recrystallization at all. Here, the strain is accumulated from pass to pass, so that the

Table II. Test Parameters

Strain/pass
ε = 0.1, 0.2, 0.3, 0.4, 0.5, 0.7
Strain rate
$\dot{\varepsilon}$ = 0.2, 2, 5, 10 s^{-1}
Interpass time
t = 5, 7.5, 10, 12.5, 15, 20, 30, 50, 80, 100, 150, 200 s

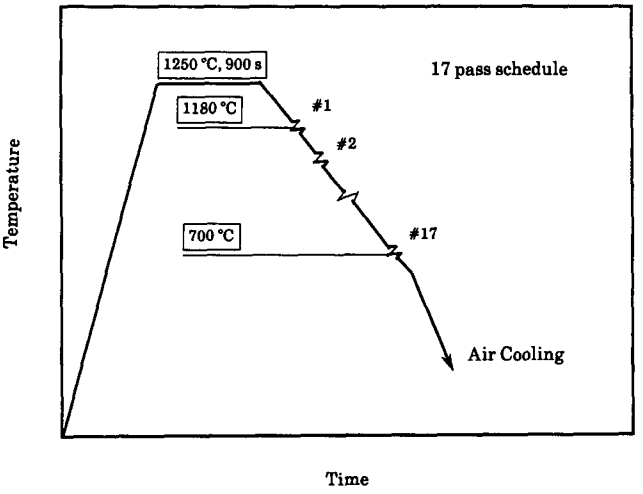

Fig. 1—Schematic representation of the schedule employed in the hot torsion tests.

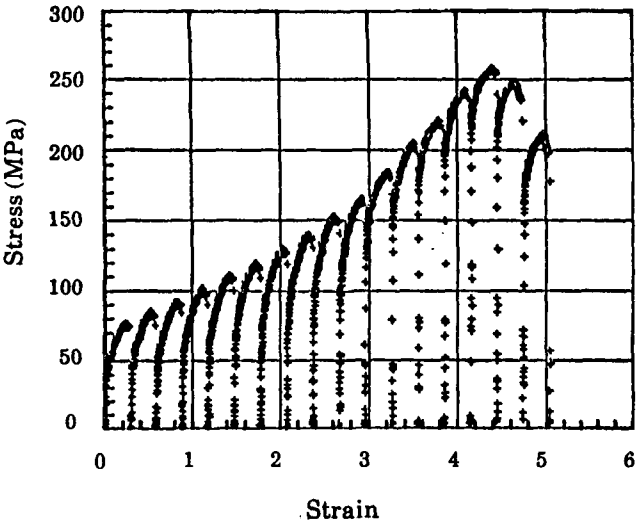

Fig. 2—Stress-strain curves for sample deformed using a 17-pass schedule.

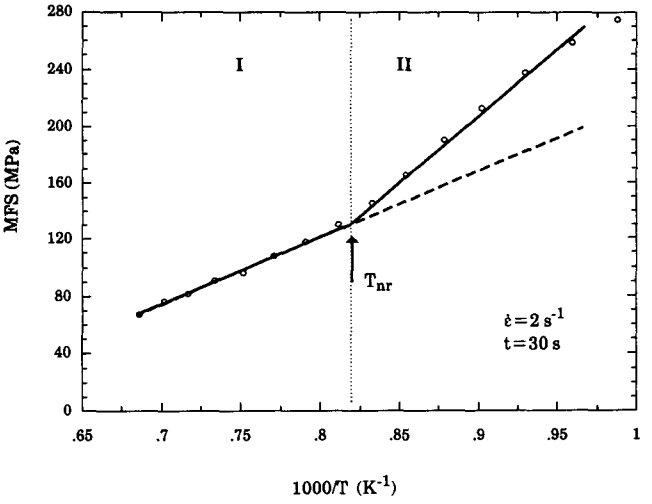

Fig. 3—Dependence of the mean flow stress (MFS) on inverse pass temperature during the multipass torsion testing of steel *B*.

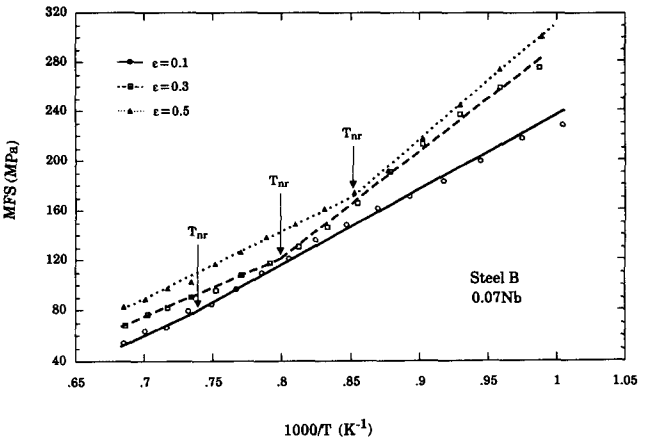

Fig. 4—Effect of pass strain on the MFS/inverse pass temperature dependence of steel *B*. Strain rate $\dot{\varepsilon} = 2\ s^{-1}$, interpass time $t = 30$ s.

mean flow stress increases more rapidly with decreasing temperature.

D. *Electron Microscopy*

In order to assess the effect of pass strain on the precipitate size distribution, two specimens of steel *C*, which had been subjected to pass strains of 0.3 and 0.7, were quenched from 972 °C and 860 °C, respectively. The effect of interpass time was assessed using specimens deformed with interpass intervals of 15, 30, 80, and 200 seconds; for this purpose, pass strains of 0.3 were employed and quenching was performed at 910 °C, after applying the ninth pass at 940 °C. The quenched specimens were polished with 1-μm diamond paste and 0.05-μm alumina, in sequence, and etched with 2 pct nital. Carbon was deposited on the etched surfaces using a vacuum evaporator in vacuums better than 5×10^{-4} torr. Squares of approximately 2 × 2 mm were scribed on the coated surfaces and removed by electropolishing using a solution of 10 pct nital; these were then mounted on copper grids for transmission electron microscope (TEM) observation.

III. RESULTS

A. *Effect of Pass Strain*

The mean flow stress *vs* $1000/T$ data for specimens tested with pass strains of 0.1, 0.3, and 0.5 are presented in Figure 4. For these tests, the strain rate and interpass time were held constant at $\dot{\varepsilon} = 2\ s^{-1}$ and $t = 30$ seconds. It can be seen from the figure that the mean flow stress increases with increasing pass strain, and that the mean flow stress slope change occurs at higher temperatures when the pass strain is reduced. This indicates that the T_{nr} decreases with increasing pass strain. Figure 5 demonstrates the dependence of the T_{nr} on pass strain for the three steels. This dependence can be described by the following relationship:

$$T_{nr} = \beta \exp(-0.36\varepsilon) \qquad [4]$$

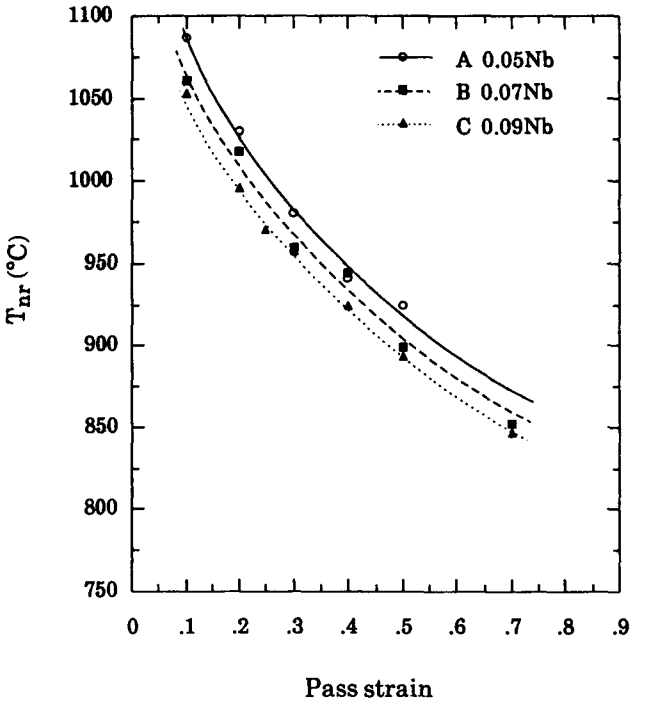

Fig. 5—Dependence of the T_{nr} on pass strain.

where β is 1103, 1088, and 1078 for steels *A*, *B*, and *C*, respectively. It can be seen that even a small change in pass strain leads to a significant change in the T_{nr}. When the strain is increased from 0.1 to 0.7, for instance, the T_{nr} in steel *B* decreases from 1060 °C to 850 °C. This is consistent with the results of Cuddy *et al.*,[17] who found that recrystallization is incomplete at about 1075 °C at pass strains of 0.04 ~ 0.13 while the temperature for complete recrystallization can be low as 925 °C when the pass strain is increased to 0.2 ~ 0.48.

Such a dramatic decrease in the T_{nr} with increasing pass strain can be due to several contributing factors.

(a) Grain refinement. When the pass strain is increased, finer grain sizes are produced by static recrystallization. Such fine structures supply more nucleation sites for subsequent recrystallization and also soften more quickly.

(b) Increased dislocation density. When the pass strain is increased, higher dislocation densities are generated, which also promotes more rapid recrystallization. When a fixed interpass time is used, this makes it possible for recrystallization to go to completion at lower temperatures.
(c) Precipitate coarsening. When the pass strain is increased, the density of dislocations increases, which leads to more rapid coarsening of the precipitates.[18] These coarsened particles lose their effectiveness in retarding recrystallization and thus allow recrystallization to continue to take place at lower temperatures.

The TEM micrographs shown in Figure 6 show the effect of increasing the pass strain on precipitate coarsening. The upper micrograph was obtained from a specimen deformed using pass strains of 0.3 and quenched at 972 °C (near the T_{nr} for this strain), while the lower micrograph represents a specimen deformed using pass strains of 0.7 and quenched at 860 °C (near the T_{nr} for the increased strain). The mean particle size in the latter case (about 110 nm) is considerably larger than in the former case (about 25 nm); these large particles are less effective in retarding recrystallization. Similar observations of precipitate coarsening during hot deformation have been reported by Weiss and Jonas[19] and Speer and Hansen.[20]

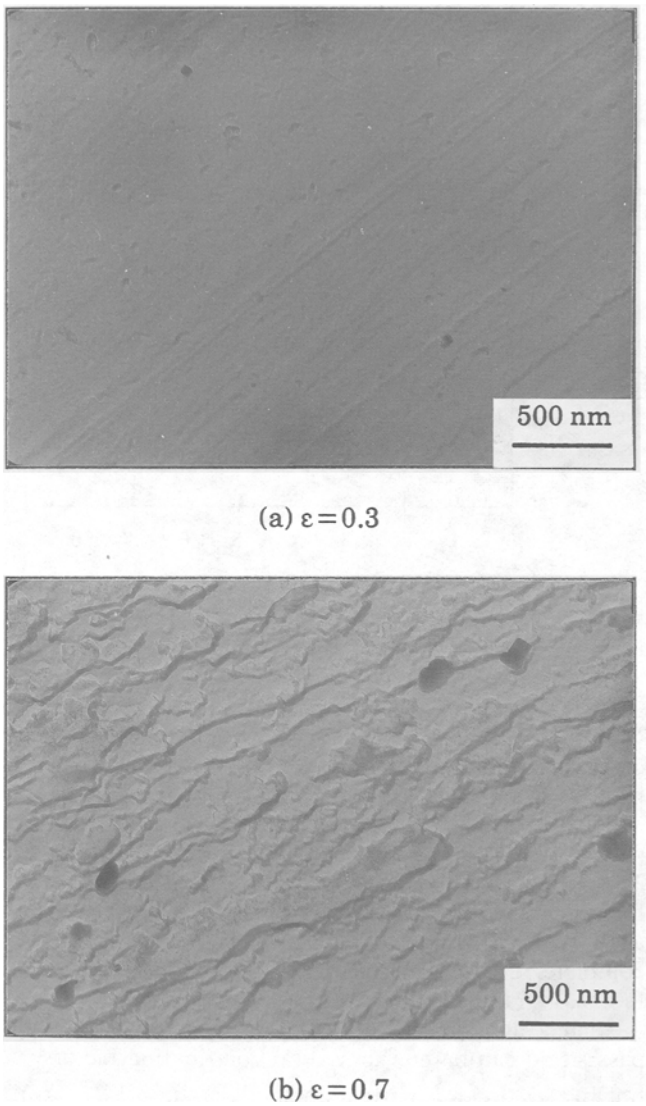

Fig. 6—Carbon extraction replicas showing the effect of strain on the precipitate morphology: (*a*) $\varepsilon = 0.3$/pass; (*b*) $\varepsilon = 0.7$/pass. Strain rate $\dot{\varepsilon} = 2\ s^{-1}$, interpass time $t = 30$ s.

B. *Effect of Strain Rate*

Some mean flow stress *vs* $1000/T$ data relating to the effect of strain rate in steel *B* are reproduced in Figure 7. For these tests, the pass strain (0.3/pass) and interpass time (30 seconds) were held constant, and only the strain rate was varied. It can be seen that the mean flow stress increases with increasing strain rate. This is because there is greater restoration by dynamic recovery at the lower strain rates. When the strain rate is 0.2 s^{-1}, for example, the deformation time for a strain of 0.3 is 1.5 seconds. By contrast, at a strain rate of $\dot{\varepsilon} = 10\ s^{-1}$, the deformation time is 0.03 seconds over the same strain interval. Such less-restored and more highly work hardened austenite supplies more driving force for static recrystallization and therefore decreases the T_{nr}.[21,22] The results presented in Figure 8 demonstrate the effect of strain rate on the T_{nr} and indicate that this phenomenon becomes more noticeable when the strain is large.

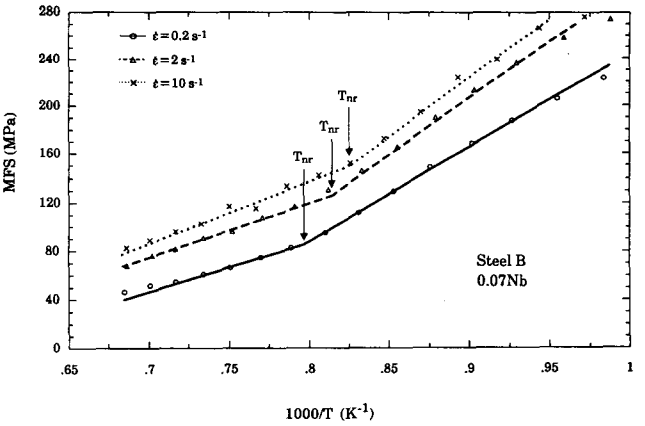

Fig. 7—Effect of strain rate on the MFS/inverse pass temperature dependence of steel *B*. Strain $\varepsilon = 0.3$/pass, interpass time $t = 30$ s.

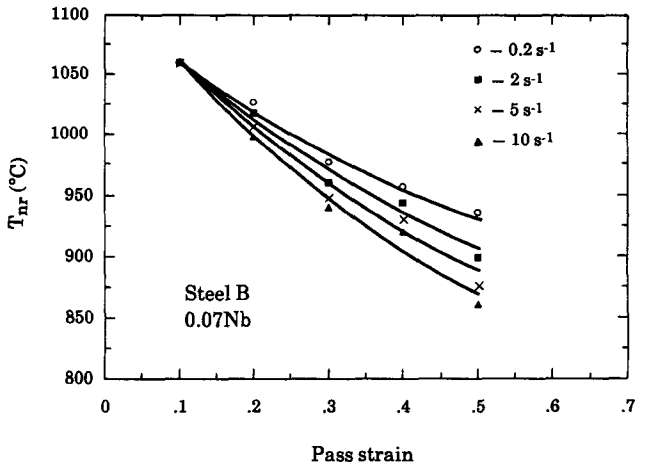

Fig. 8—Effect of strain rate on the T_{nr}.

C. *Effect of Interpass Time*

Some mean flow stress *vs* $1000/T$ data illustrating the effect of interpass time in steel *B* are presented in Figure 9. For these tests, the pass strain (0.3/pass) and strain rate ($\dot{\varepsilon} = 2\ s^{-1}$) were held constant and the interpass time was increased from 5 to 150 seconds. At temperatures above the T_{nr}, the interpass time does not affect the mean flow stress because full recrystallization takes place between passes and there is no precipitation. Thus, the mean flow stress is only a function of temperature and grain size.

At the temperatures below the T_{nr}, precipitation takes place, so that the increase in mean flow stress is attributable not only to the decrease in temperature but also to the retardation of recrystallization by precipitation (*i.e.*, to increases in the retained strain). At temperatures close to the nose of the precipitation-temperature-time (PTT) curve, longer interpass times lead to precipitate coarsening, which weakens the retarding effect of precipitation, and no T_{nr} is observed. At still lower temperatures, the rate of coarsening is reduced and the T_{nr} can once again be detected, even when the interpass times are long. This is why the mean flow stresses for interpass times of 150 seconds are lower in Figure 9 than for interpass times of 5 seconds at temperatures below the T_{nr}.

The dependence of T_{nr} on interpass time is illustrated in Figure 10 for steel *B*. It can be divided into three distinct regions: short interpass times ($t < 12.5$ seconds), medium interpass times ($12.5 < t < 80$ seconds), and long interpass times ($t > 80$ seconds). In the range of short interpass times (region I), precipitation is unable to take place, so that only solute drag is available for the retardation of recrystallization.[23] In this range, the extent of recrystallization increases with increasing interpass time, thus decreasing the T_{nr}. With further increases in interpass time, if no precipitation were to take place, the T_{nr} would decrease continuously along the broken curve. For the present steels, however, when the interpass time is increased over a critical value (for instance, 12.5 seconds for steel *B*), precipitation takes place and the retardation of recrystallization is mainly attributable to precipitation, so that the T_{nr} shifts to the solid curve in this range. In the third region, the interpass times are so long (>80 seconds) that precipitate coarsening begins to play a role and the retardation of recrystallization by precipitation is weakened. This causes the T_{nr} to decrease again.

Some typical TEM micrographs corresponding to experiments on steel *B* with increasing interpass times are presented in Figure 11. The quenching temperature was 910 °C in all these cases. It can be seen that when the interpass time was increased from 5 to 200 seconds, the mean particle size increased from 15 to 135 nm. It is evident from the final micrograph that the particle density has decreased, indicating that coarsening is taking place. These micrographs are thus consistent with the interpretation given to the mechanical results in this section and supports the explanation proposed.

The dependence of the T_{nr} on the interpass time in the range of short holding intervals is presented in Figure 12 for steels *A* and *C*. The steel *B* results of Figure 10 are included in this figure for comparison purposes. It is evident that precipitation is slightly more rapid in steels *A* and *B*. In the case of steel *A*, this is because it has a higher solubility product for C, N, and Nb than the other grades and therefore a higher level of supersaturation at a given deformation temperature. In steel *B*, the higher level of titanium concentration (0.026 wt pct) leads to Ti(C,N) precipitation; these particles act as nucleation sites for Nb(C,N) precipitation[24,25,26] and therefore retard recrystallization in this way. In the short interpass time region, in which solute drag controls the rate of recrystallization, the order of the T_{nr} for these steels is *B*, *C*, *A*; this is because steel *B* contains the highest concentration of Nb plus Ti, whereas the lowest is found in steel *A*.

IV. DISCUSSION

A. *Kinetics of Recrystallization and Precipitation*

Approximate predictions of the T_{nr} can be obtained from the intersections of the $t_{0.05p}$ (time for 5 pct precipitation)

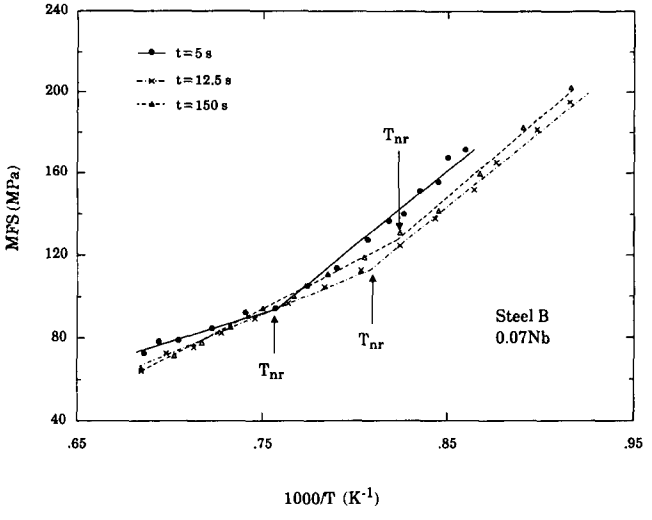

Fig. 9—Effect of interpass time on the MFS/inverse pass temperature dependence of steel *B*. Strain $\varepsilon = 0.3$/pass, strain rate $\dot{\varepsilon} = 2\ s^{-1}$.

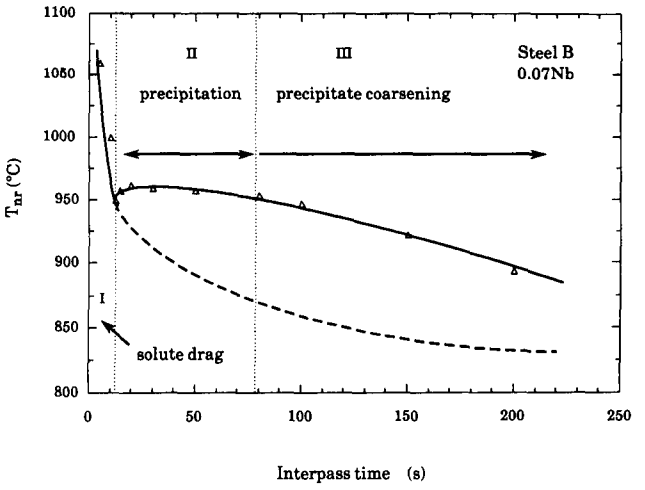

Fig. 10—The three ranges of interpass time dependence of the T_{nr} (steel *B*).

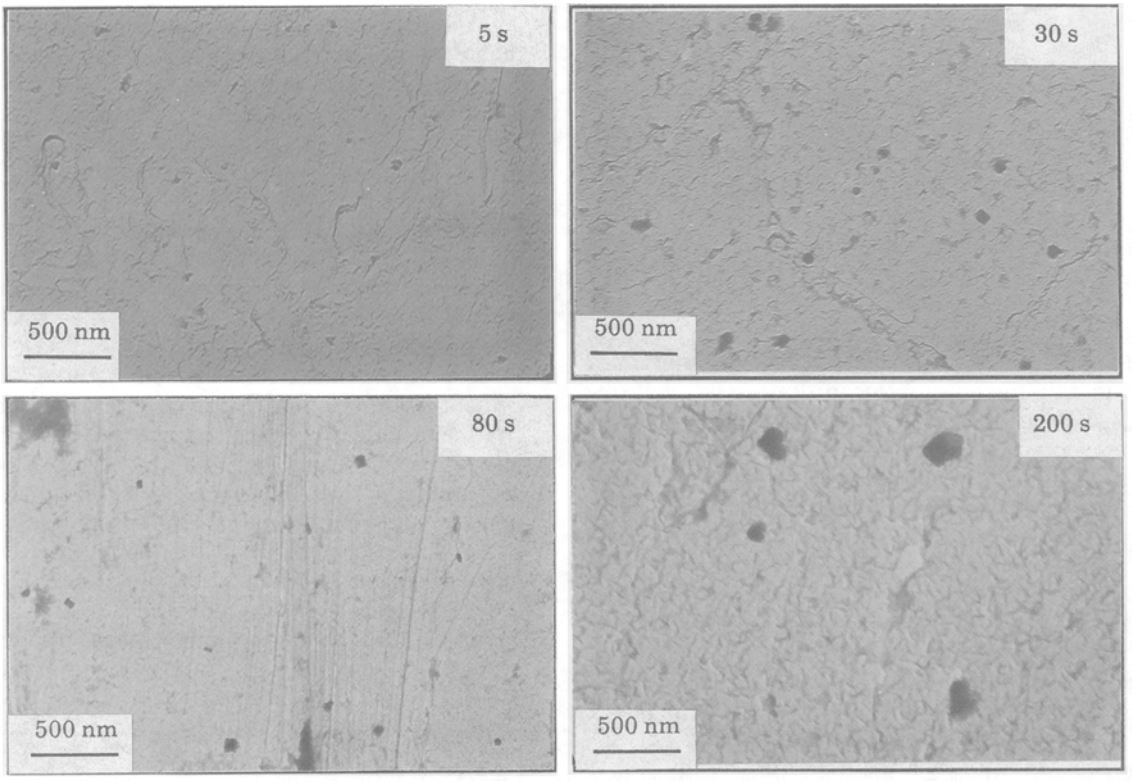

Fig. 11—Effect of interpass time on precipitate morphology in steel *B*. Samples were quenched from 910 °C.

and $t_{0.95x}$ (time for 95 pct recrystallization) curves in the Dutta and Sellars recrystallization and precipitation models.[27] These were calculated as follows:

$$t_{0.05p} = A\varepsilon^{-1} \qquad [5a]$$

where

$$A = 3 \times 10^{-6} [Nb]^{-1} Z^{-0.5} \times \exp\frac{270{,}000}{RT} \exp\frac{2.5 \times 10^{10}}{T^3 (\ln ks)^2} \qquad [5b]$$

and

$$t_{0.95x} = B\varepsilon^{-4} \qquad [6a]$$

where

$$B = 7.64 \times 6.75 \times 10^{-20} d_0^2 \times \exp\frac{300{,}000}{RT} \exp\left\{\left(\frac{2.75 \times 10^5}{T} - 185\right)[Nb]\right\} \qquad [6b]$$

Here, [Nb] is the concentration of niobium in solution, Z is the Zener-Hollomon parameter, and k_s is the supersaturation ratio which is, in turn, given by

$$k_s = \frac{[Nb][C + 12/14\, N]_{soln}}{10^{2.26-6770/T}} \qquad [7]$$

where C and N refer to the concentrations of these elements in solution in the austenite. The dependences of $t_{0.05p}$, $t_{0.05x}$ (time for 5 pct recrystallization), and $t_{0.95x}$ on strain at a deformation temperature of 960 °C and a strain rate of 2 s^{-1} are illustrated in Figure 13 for steel *C*. For the construction of this figure, the ratio $t_{0.95x}/t_{0.05x}$ was taken as 7.64, which was calculated from the Avrami equation using an exponent $n = 2$.[28]

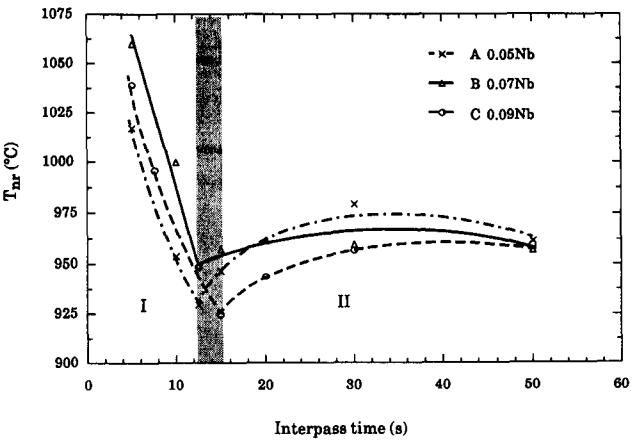

Fig. 12—Effect of interpass time on the T_{nr} in steels *A*, *B*, and *C*.

It can be seen that the $t_{0.05p}$ (precipitation) curve intersects the $t_{0.05x}$ and $t_{0.95x}$ (recrystallization) curves at $\varepsilon_1 = 0.27$ and $\varepsilon_2 = 0.43$, respectively. Thus, for values of $\varepsilon < 0.27$, precipitation is initiated before recrystallization, and $t_{0.05x}$ and $t_{0.95x}$ are shifted to much longer times. In the strain range 0.27 to 0.43, $t_{0.05p}$ is greater than $t_{0.05x}$ but less than $t_{0.95x}$; this means that recrystallization is initiated before precipitation, but its completion will be delayed by precipitation. Finally, when $\varepsilon > 0.43$, $t_{0.05p}$ is greater than both $t_{0.05x}$ and $t_{0.95x}$, so that

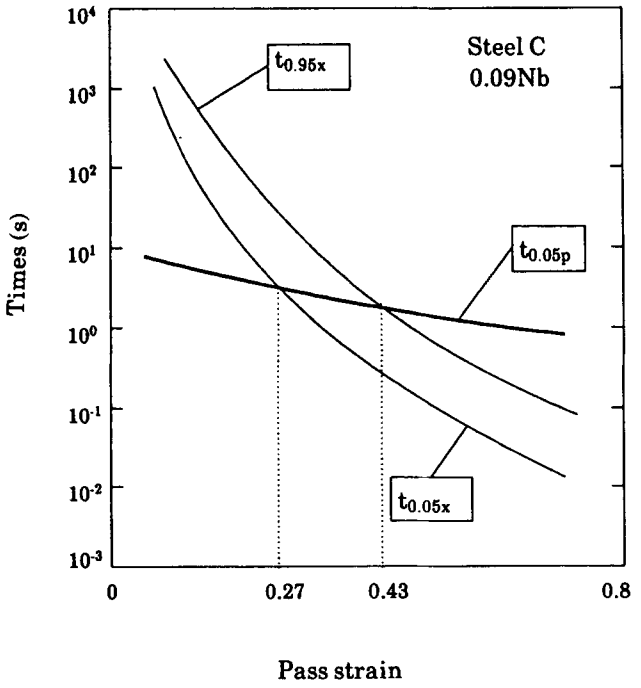

Fig. 13—Influence of pass strain on $t_{0.05p}$, $t_{0.05x}$, and $t_{0.95x}$ at 960 °C.

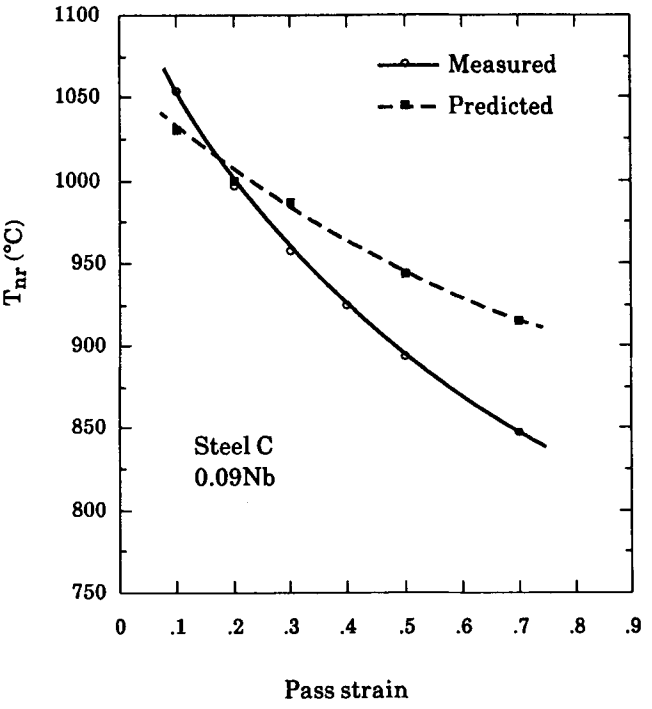

Fig. 14—Comparison between the T_{nr}'s determined in the present experiments and those predicted using the Dutta and Sellars (isothermal) model.

recrystallization is completed before precipitation can be initiated. In summary, if $t_{0.05x} > t_{0.05p}$, precipitation is initiated before recrystallization; otherwise, recrystallization is initiated before precipitation.

The rates of change of $t_{0.05p}$ and $t_{0.95x}$ with strain can be obtained from the first derivatives of Eqs. [5a] and [6a] with respect to strain:

$$\frac{\partial(t_{0.05p})}{\partial\varepsilon} = -A\varepsilon^{-2} \quad [8]$$

$$\frac{\partial(t_{0.95x})}{\partial\varepsilon} = -4B\varepsilon^{-5} \quad [9]$$

From Eqs. [8] and [9], it can be seen that the recrystallization kinetics are more sensitive to strain than the precipitation kinetics, although the difference diminishes as the strain approaches unity. Thus, T_{nr} decreases continuously with strain, as in Figure 5, where the T_{nr} decreases by 57 °C (from 1053 °C to 996 °C) when the strain is increased from 0.1 to 0.2. When the strain is increased from 0.2 to 0.4, the T_{nr} decreases by a further 71 °C (from 996 °C to 925 °C).

B. *Prediction of the T_{nr}*

The Dutta and Sellars model was derived for isothermal conditions, so that an error is likely to be introduced when it is applied to the continuous cooling conditions prevailing in industry. The T_{nr}'s determined in the present investigation are therefore compared with the T_{nr}'s predicted using the Dutta and Sellars model in Figure 14. It is apparent that the difference between the measured and predicted T_{nr}'s is largest at large strains. In order to throw some light on this discrepancy, some calculations were performed using the additivity rule to predict the continuous cooling behavior from isothermal data. These calculations are described in Section IV–B–2.

1. *The additivity rule*

The additivity rule has been shown to lead to predictions of the continuous-cooling-transformation (CCT) behavior from isothermal-transformation (IT) data that are in reasonable agreement with experimental results in the case of the proeutectoid ferrite, pearlite, and bainite transformations.[29,30] Park *et al.*[31] have also applied the additivity rule successfully to calculate the continuous-cooling-precipitation (CCP) curve from isothermal (PTT) data. Since recrystallization is a kind of phase transformation, it should be possible to predict the continuous-cooling-recrystallization (CCR) behavior using the same rule. This calculation was performed in the present study using the relation.[32]

$$\int_{Te}^{T} \frac{1}{\tau_x(T_i)} \frac{dt}{dT} dT = 1 \quad [10]$$

Here $\tau_x(T_i)$ is the time at which the reaction is x pct complete at a temperature T_i, dt/dT is the inverse of the cooling rate, and T_e is the equilibrium temperature at which the reaction is initiated.

2. *Calculation of CCR and CCP curves*

The following assumptions were made in this case: (1) after each deformation, the occurrence of recrystallization and precipitation can be modeled separately; and (2) at the ith pass, the deformation temperature can be used in place of T_e in Eq. [10].

The cooling curves were divided into 0.01 °C increments, and τ_x and Δt_i were calculated at each temperature. The recrystallization finish and precipitation start

times for each pass were then evaluated from the times when the sums of the reaction time ratios $\Delta t_i/\tau_x$ reached unity.

For calculation of the recrystallization finish time ($t_{0.95x}$) at the ith pass, the recrystallized grain size at the $(i-1)$-th pass was taken equal to the initial grain size at the ith pass. It can be evaluated from the relation[33]

$$d_i = D d_{i-1}^{0.67} \varepsilon^{-0.67} \quad [11]$$

where D is a constant taken as 1.6 and 1.1 for steels A and C, respectively. The recrystallization-precipitation-temperature-time (RPTT) diagrams obtained in this way for steel C are presented in Figure 15. The broken curves represent $t_{0.95x}$, and the solid ones represent $t_{0.05p}$. The arrows identify the points of intersection of the $t_{0.95x}$ and $t_{0.05p}$ curves. The temperatures that correspond to these points are the predicted T_{nr}'s, and the steel A and C results are presented as examples in Figure 16. It is evident that by correcting for the continuous cooling conditions pertaining to the present experiments, the agreement between the predicted and measured T_{nr}'s is improved considerably.

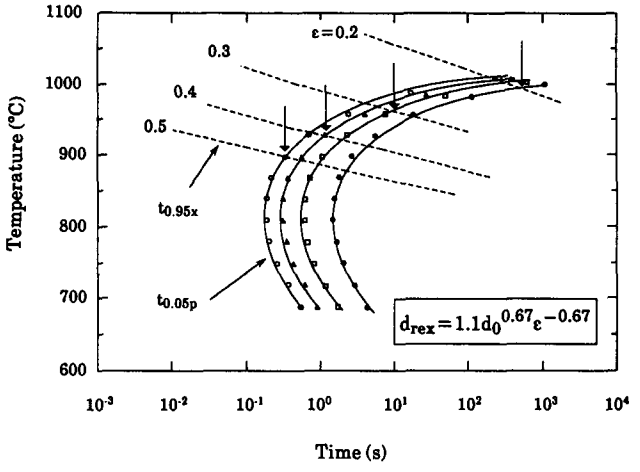

Fig. 15—RPTT diagrams calculated for continuous cooling–multipass deformation conditions. Arrows identify the T_{nr} pertaining to each pass strain.

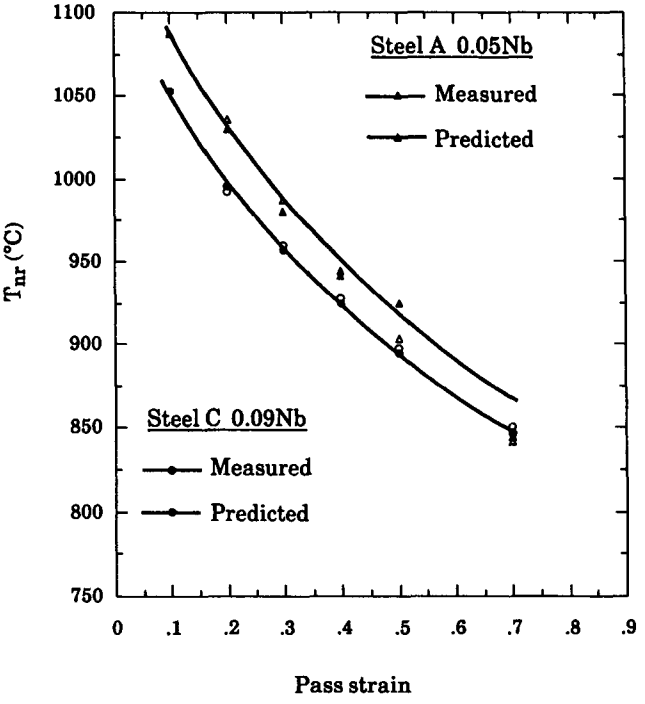

Fig. 16—Effect of pass strain on the measured and predicted T_{nr}'s in steels A and C.

V. CONCLUSIONS

1. The T_{nr} decreases significantly with increasing strain. At a pass strain of 0.7, for example, the measured T_{nr} can be less than 850 °C. Such low T_{nr}'s result from the following: (1) the significant grain refinement of austenite by successive recrystallizations; (2) the acceleration of recrystallization by the higher dislocation densities produced by the larger strains; and (3) the strain induced coarsening of the precipitates.
2. In the range of temperatures where strain induced precipitation is likely to occur, both recrystallization and precipitation are accelerated when prestraining is carried out at high strain rates. Because the recrystallization kinetics are more sensitive to strain rate than the precipitation kinetics, the T_{nr} is decreased in this way.
3. The influence of interpass time on the T_{nr} can be divided into three regions. When the interpass times are short (<12 seconds), recrystallization is retarded by solute drag and the T_{nr} decreases with increasing interpass time. For interpass times in the 12 to 50 second range, the T_{nr} increases with increasing interpass time because of the increasing volume fraction of fine precipitates. When the interpass times are increased beyond 50 seconds, however, precipitate coarsening takes place, which leads to a decrease in the T_{nr}.
4. By applying the additivity rule to the isothermal model of Dutta and Sellars, continuous cooling T_{nr}'s can be predicted from RPTT diagrams. The T_{nr} predictions obtained in this way are in good agreement with experimental data determined under continuous cooling conditions.

ACKNOWLEDGMENTS

The authors are indebted to Stelco Inc. for supplying the experimental materials. They would also like to express their special appreciation to Drs. C. Roucoules and P.R. Cetlin for their useful suggestions. The financial support received from the Natural Sciences and Engineering Research Council of Canada (NSERC) and the Canadian Steel Industry Research Association (CSIRA) is acknowledged with gratitude. One of the authors (DQB) is indebted to the Ministry of the Aerospace Industry, China, for providing a visiting fellowship.

REFERENCES

1. W.J. Liu and J.J. Jonas: *Metall. Trans. A*, 1988, vol. 19A, pp. 1403-13.
2. W.P. Sun, W.J. Liu, and J.J. Jonas: *Metall. Trans. A*, 1989, vol. 20A, pp. 2707-15.

3. B. Migaud: *Hot Working and Forming Processes*, C.M. Sellars and G.J. Davis, eds., Sheffield, England, 1979, pp. 67-76.
4. L.N. Pussegoda, S. Yue, and J.J. Jonas: *Metall. Trans. A*, 1990, vol. 21A, pp. 153-64.
5. L.N. Pussegoda and J.J. Jonas: *Iron Steel Inst. Jpn. Int.*, 1991, vol. 31 (3), pp. 278-88.
6. F.H. Samuel, S. Yue, J.J. Jonas, and B.A. Zbinden: *Iron Steel Inst. Jpn. Int.*, 1989, vol. 29 (10), pp. 878-86.
7. F.H. Samuel, S. Yue, J.J. Jonas, and K.R. Barnes: *Iron Steel Inst. Jpn. Int.*, 1990, vol. 30 (3), pp. 216-25.
8. F. Boratto, R. Barbosa, S. Yue, and J.J. Jonas: *THERMEC-88*, Imao Tamura, ed., Tokyo, Japan, 1988, vol. 1, pp. 383-90.
9. S. Yue and J.J. Jonas: *Mater. Forum*, 1990, vol. 14, pp. 245-52.
10. D.Q. Bai, S. Yue, W.P. Sun, and J.J. Jonas: *Processing, Microstructure and Properties of Microalloyed and Other Modern Low Alloy Steels*, Proc. Int. Conf., A.J. DeArdo, ed., Pittsburgh, PA, June 4–6, 1991, pp. 165-73.
11. D.Q. Bai, S. Yue, W.P. Sun, and J.J. Jonas: *34th Mechanical Working and Steel Processing*, Proc. Int. Conf., Montreal, Oct. 1992, pp. 515-23.
12. L.M. Brown and W.M. Stobbs: *Phil. Mag.*, 1971, vol. 23, p. 1201.
13. P.F. Chapman and W.M. Stobbs: *Phil. Mag.*, 1969, vol. 19, p. 1015.
14. T.C. Rollason and J.W. Martin: *J. Mater. Sci.*, 1970, vol. 5, p. 127.
15. T. Chandra, S. Yue, J.J. Jonas, and R.J. Ackert: in Proc. 4th Int. Conf. on The Science and Technology of Flat Rolling, Deauville, France, June 1987, vol. 2, pp. F.18.1-F.18.8.
16. K.J. Irvine, F.B. Pickering, and T. Gladman: *J. Iron Steel Inst.*, 1967, vol. 205, pp. 161-82.
17. L.J. Cuddy, J.J. Bauwin, and J.C. Raley: *Metall. Trans. A*, 1980, vol. 11A, pp. 381-86.
18. W.P. Sun, M. Militzer, and J.J. Jonas: *Metall. Trans. A*, 1992, vol. 23A, pp. 3013-23.
19. I. Weiss and J.J. Jonas: *Metall. Trans. A*, 1980, vol. 11A, pp. 403-10.
20. J.G. Speer and S.S. Hansen: *Metall. Trans. A*, 1989, vol. 20A, pp. 25-38.
21. D.R. Barraclough and C.M. Sellars: *Met. Sci.*, 1979, vol. 13, pp. 257-67.
22. E. Ruibal, J.J. Urcola, and M. Fuentes: *Z. Metallkde*, 1985, vol. 76, p. 568.
23. W.P. Sun, M. Militzer, D.Q. Bai, and J.J. Jonas: *Recrystallization '92*, Materials Science Forum, 1992, vols. 113–115, pp. 533-38.
24. S.V. Subramanian, F. Boratto, J.J. Jonas, and C.M. Sellars: *Microalloyed Bar and Forging Steels*, M. Finn, ed., Hamilton, ON, Canada, 1990, pp. 120-36.
25. H.L. Zou and J.S. Kirkaldy: *Metall. Trans. A*, 1991, vol. 22A, pp. 1511-23.
26. M. Djahazi, X.L. He, J.J. Jonas, and W.P. Sun: *Metall. Trans. A*, 1992, vol. 23A, pp. 2111-20.
27. B. Dutta and Sellars: *Mater. Sci. Technol.*, 1987, vol. 3, pp. 197-206.
28. D.Q. Bai: Master's Thesis, McGill University, Montreal, PQ, Canada, 1992.
29. M. Umemoto, K. Horiuchi, and I. Tamura: *Trans. Iron Steel Inst. Jpn.*, 1982, vol. 22, pp. 854-61.
30. M. Umemoto, K. Horiuchi, and I. Tamura: *Trans. Iron Steel Inst. Jpn.*, 1983, vol. 23, pp. 690-95.
31. S.H. Park, S. Yue, and J.J. Jonas: *Metall. Trans. A*, 1992, vol. 23A, pp. 1641-51.
32. E. Scheil: *Arch. Eisenhüttenwes.*, 1935, vol. 12, pp. 565-67.
33. C.M. Sellars: *Hot Working and Forming Processes*, C.M. Sellars and G.J. Davies, eds., Sheffield, England, 1979, pp. 3-15.